RSC Advances

REVIEW

View Article Online
View Journal | View Issue

Cite this: *RSC Adv.*, 2022, **12**, 24946

Recent progress of Ga-based liquid metals in catalysis

Xi Sun and Hui Li *

Within the last decade, the application of gallium-based liquid metals in catalysis has received great attention from around the world. This article provides an overview concerning Ga-based liquid metals (LMs) in energy and environmental applications, such as the catalytic synthesis of ethylene by non-petroleum routes *via* Pd–Ga liquid catalysts, alkane dehydrogenation *via* Pd–Ga or Pt–Ga catalysts, CO_2 hydrogenation to methanol *via* Ni Ga or Pd/Ga_2O_3 catalysts, and catalytic degradation of CO_2 *via* EGaIn liquid metal catalysts below 500 °C, where Ga-based liquid metal catalysts exhibit high selectivity and low energy consumption. The formation of isolated metal sites in a liquid metal matrix allows the integration of several characteristics of multiphase catalysis (particularly the operational friendliness of product separation procedures) with those of homogeneous catalysis. In the end, this article sheds light on future prospects, opportunities, and challenges of liquid metal catalysis.

Received 1st August 2022
Accepted 25th August 2022

DOI: 10.1039/d2ra04795k

rsc.li/rsc-advances

1 Introduction

Typically, liquid metal catalysts are utilized in reactions where the reaction temperature exceeds the catalyst's melting point. Several metals with low melting points including gallium (Ga), mercury (Hg), cesium (Cs), rubidium (Rb), and francium (Fr) have been favored by researchers. As the most widely studied liquid metals, Ga and Ga-based liquid metal alloys have been considered as a new class of composite materials in many fields. While retaining the excellent electrical and thermal conductivity of conventional metals, liquid metal is the softest of all conductive substances.[1] In contrast to Hg, a common liquid metal whose toxicity limits its research and applications, the biocompatibility and near-zero vapor pressure of Ga and Ga-based liquid metal alloys make Ga-based liquid metals promising for research in a variety of fields.[2]

As a liquid phase metal, Ga functions as a metal solvent, and the proportions of different metals associated with Ga metal can be adjusted to create alloys with varying melting points. Gallium–Indium alloys (EGaIn) and Gallium–Indium–Tin alloys (Galinstan) are two commonly used liquid metals based on Ga.[3–5] The

Dalian Institute of Chemical Physic, CAS, Dalian 116023, China. E-mail: hui.li@dicp.ac.cn

Xi Sun received his Bachelor's degree in Environmental Science and Engineering from Liaoning Technical University, and is now working on liquid metal alloy catalyst performance evaluation, advanced catalysis materials, green hydrogen, methane/ammonia production, and high purity hydrogen separation and compression.

Professor Hui Li received his PhD in Industrial Catalysis from University of Chinese Academy of Sciences. He was awarded an Outstanding Overseas Youths award and has long been engaged in basic research on the application of palladium membrane purification materials in fuel cell hydrogen sources and large-scale hydrogen purification, and catalytic carbon conversion to higher-value products. As the project leader, he has led 10 projects, including the EU 6th and 7th framework studies, and achieved the first industrial-scale demonstration of ultra-pure hydrogen purification (800 nm3 h^{-1}) and a methane reforming palladium membrane reactor for IGCC.

melting points of these two alloys (≈11 °C, ≈−19 °C) are even lower than pure Ga (29.78 °C).[4] A bimetallic or even polymetallic catalyst has greater catalytic activity than its monometallic counterpart due to the synergistic effect.[6] Liquid metals composed of Ga tend to oxidize since Ga in contact with oxygen (O) forms a nanometer-thick layer of dense, smooth metal oxide on the surface of the metal, which is partially passivated and prevents further oxidation of the metal from inside.[7] Using electrochemical methods, it is possible to manipulate the oxide species on the surface by adjusting the composition of the liquid metal or by regulating the gain or loss of electrons.[8] Under the protection of Ga, this property enables numerous active metal catalysts to increase their catalytic activity.[9] This article reviews main research advancements in Ga-based liquid metal applications in energy and environmental catalysis fields, and shed light on opportunities and challenges for future developments.

2 Categories, synthesis and fabrication

2.1 Ga–Pd bimetallic catalysts

It is possible to modify the catalytic properties of LM by dissolving noble metals or transition metals to form intermetallic compounds. Modifying the electronic structure of supported LM catalysts can alter their catalytic properties. Gallium–palladium (Ga–Pd) bimetallic catalysts are superior liquid catalysts when compared to Pd or Ga catalysts alone. According to Fig. 1(a), GaPd, $GaPd_2$, and Ga_7Pd_3 have good crystal structures, exhibiting superior electronic properties compared to the pure metal, thereby enhancing the catalytic selectivity, long-term operational stability, and catalytic performance of these catalysts in reduction or oxidation reactions.[10]

Ga–Pd nanoparticles were synthesized in an inert atmosphere by dissolving palladium acetylacetonate (Pd $(acac)_2$) in tetrahydrofuran (THF) with heating and stirring, dissolving gallium trichloride ($GaCl_3$) in lithium triethyl borohydride ($LiHBEt_3$) and then pumping it into the THF solution to produce a black suspension, with prolonged stirring of the suspension. Then a centrifuge was used to separate the solid from the liquid. After the separation and three repeated THF rinses, the black solid sediment was extracted and dried. To ensure the formation of intermetallic compounds, the dried precipitate particles were re-dissolved in dioctyl ether for four hours with heating and stirring, and the washing and drying processes were repeated after solid–liquid separation.[11,12]

2.2 Ga–Pt bimetallic catalysts

In the hydrogenation catalytic reactions, Pt catalysts get reduced to electron deficent Pt species,[13] the inclusion of gallium creates Pt–Ga assemblies such as gallium–Pt alloys on the catalyst surface, with Pt–Ga interactions. Previous work has demonstrated that iron, tin, and germanium successfully boosted the catalytic performance of Pt catalysts.[14–17] The addition of gallium significantly increases the dispersion of platinum[18] and exhibits increased exposure of platinum active sites on the catalyst surface to the reaction atmosphere. The platinum–gallium interaction also changes the electronic structure around the platinum atom and alters the electronic properties of the platinum active center,[19] with implications for properties such as the selectivity of the Pt catalyst.[20,21]

The electrocoupling substitution method can be used to prepare Ga–Pt SCALM catalysts[13]. First, pure Ga was heated and stirred in an isopropanol solvent to form a Ga suspension. Next, an aqueous solution of chloroplatinic acid was added to the Ga suspension, which was obtained through evaporation and calcination. Platinum acetylacetonate (Pt $(acac)_2$) was added to a toluene solution, evaporated from the toluene at 453 K, and calcined at 923 K for three hours in air, according to a second method. *In situ* XRD or catalytic measurements are capable of reducing the resulting catalyst to form Pt monometallic and/or Pt–Ga bimetallic nanoparticles on its surface.[22]

2.3 Ga–Ni bimetallic catalysts

Nickel nitrate hexahydrate ($Ni(NO_3)_2 \cdot 6H_2O$) and Ga metal were utilized to create Ni–Ga catalysts by means of stepwise evaporation co-condensation (sol–gel method) and reflux co-condensation techniques. The method of preparation was as follows. Ga metal was completely dissolved in a nitric acid solution to produce $Ga(NO_3)_3$. The acid mixture was neutralized and precipitated in excess with a concentrated NaOH solution until its pH ranged from 9.5 to 10. Utilizing a heater for 24 hours, the temperature of the mixture was increased to a range of temperatures. After 24 hours, the process was to gradually evaporate the water by removing the reflux system, and the mixture was in gel form. The gel was washed and filtered until its pH became neutral and it solidified into a moist substance. The product was dried overnight at 100 °C, followed by a six-hour calcination process at 500 °C to produce white powders and calcined samples. By adding calcined samples to a $NaBH_4$ solution in anhydrous ethanol, the mixed oxides of Ni^{2+} and Ga^{3+} were converted into Ni–Ga alloys with different Ni/Ga molar ratios.[23]

Alternatively, the urea hydrolysis hydrothermal method was used to fabricate the Ni_5Ga_3 catalyst by preparing a hydrogen-like compound (HTlc) precursor with 65% nickel atom and gallium equilibrium. $Ni(NO_3)_2$–$6H_2O$ and $Ga(NO_3)_3$–$9H_2O$ were dissolved in 50 mL of distilled water at 65–35% molar percentages, and urea in the same nitrate ratio was then dissolved in the aqueous solution under strong stirring. Different samples of the prepared mixture were sealed in a hydrothermal reactor at 90 °C, 110 °C, 130 °C and 150 °C to study the effect of synthesis temperature. The products were maintained for 16 h, followed by centrifugation, washing with deionized water and drying at 100 °C overnight to obtain the HTlc precursor. The dry cake x-HTlc produced above was crushed and sieved with 40–60 mesh, and the collected sample was reduced in a tube furnace at a heating rate of 5 °C min^{-1} in a mixture of 5% H_2 and Ar at an equilibrium temperature of 40 mL min^{-1} for 6 h. The corresponding reduced metal alloy was denoted as x-Ni_5Ga_3.[24]

2.4 EGaIn and Galinstan liquid metal catalysts

Gallium readily alloys with many metals.[25] Therefore, as a component, gallium can potentially serve to form a variety of

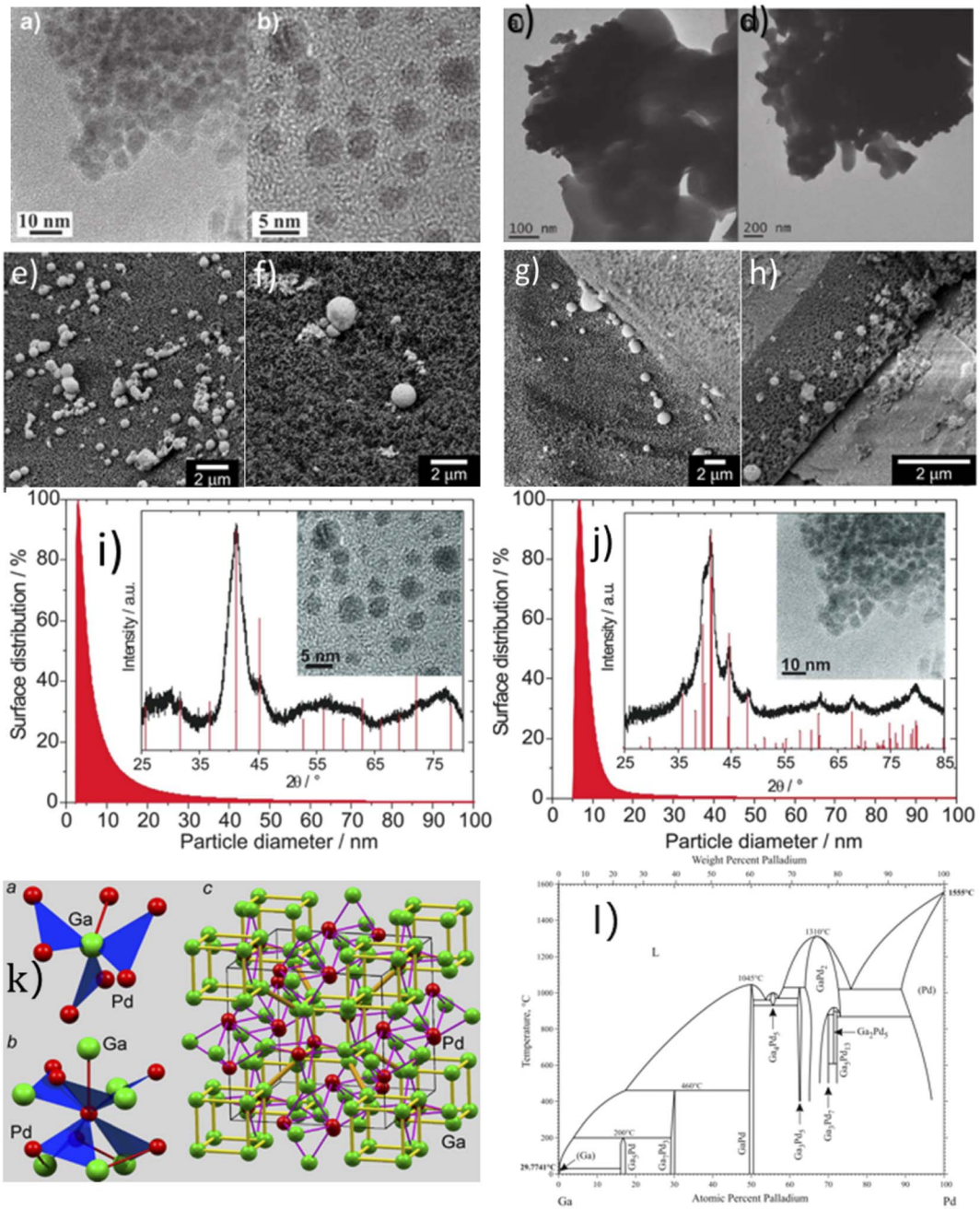

Fig. 1 TEM images of Ga–Pd nanoparticles: (a) $GaPd_2$ cluster particles, 3–7 nm diameter; (b) GaPd nanoparticles, 1–5 nm diameter; SEM images of (c) $GaPd_2$ and (d) GaPd loaded on alumina carriers; (e) SEM images of pure Ga-modified porous glass. (f and g) Pd/Ga = 10 samples before reaction; (h) Pd/Ga sample 20 h post-reaction; (i) GaPd particle size distribution measured by disk centrifuge, TEM image, and XRD image with a theoretical histogram of nanoparticles; (j) $GaPd_2$ particle size distribution measured by disk centrifuge, TEM image, and XRD image with theoretical histograms; (k) chemical bonding analysis plots in GaPd and Ga_7Pd_3; (l) Ga–Pd phase diagram.

low melting point alloys with other metals, including indium (In),[26] lead (Pb),[27] bismuth (Bi), tin (Sn),[28] aluminum (Al), zinc (Zn),[29] *etc.* The melting point of alloys varies depending on the composition and ratio.

EGaIn and Galinstan are metals with melting points below or close to room temperature. The EGaIn alloy was produced by combining Ga and In in stoichiometric proportions (75.5 wt% Ga and 24.5 wt% In).[30] The constituent metals were mixed in a thermoset on a heating plate at approximately 200 °C (above the melting point of iron) until completely dissolved and thoroughly combined, and the alloy was allowed to cool naturally.[31] Similarly, the GaSnIn alloy was produced by melting 68.5 wt% Ga, 21.5 wt% In and 10 wt% Sn [30] in a heated beaker, stirring thoroughly, and then cooling the metal.[32] Liquid metals as such could even be dispersed into nanoparticles towards multiple functions, as can be done by a simple sonication method in the

presence of organic solvents.[33] First, a certain quantity of liquid metal bulk in a vessel containing thiol ethanol solution is added and an ultrasonic probe is applied to introduce cavitation in the solution, and the liquid metal bulk stabilized by the oxide layer is rapidly fractured into numerous liquid metal nanoparticles by oscillatory shear force. This results in local extremes of pressure and temperature in an ultrashort period of time. In this case, thiolated ligands can be assembled easily and firmly on the surface of nascent liquid metal nanoparticles at the same time, competing with the oxidation process of liquid metal. Eventually, spherical liquid metal nanoparticles are formed under continuous sonication and are stabilized due to the protection of thiol ligands and the rapid oxidation of the surface.[34,35]

2.5 Liquid metal/metal oxides (LM/MO) framework and Au/Ag-Galinstan liquid metal framework catalysts

Solid metal/metal oxide (SM/MO) are of tremendous interest due to their unique physicochemical characteristics of its micro- and nanostructures.[36–39] Comparing to SM/MO, LM/MO exhibits additional dimensions to the structure, with the flexibility, the possibility of mixing with other metals and their recyclability, fluidity, and high conformation.[40]

Liquid metal framework, which consists of solid metal nanoparticles (primarily precious or transition metal species) encased in a liquid metal framework, augments the catalytic activity of solid catalysts.[41] The Au/Ag-Galinstan catalysts were synthesized using a galvanic replacement reaction. For 72 h, droplets of Galinstan were immersed in 0.1–5 mM aqueous solutions of varying concentrations of $AgNO_3$ or $KAuBr_4$, or in 0.1–1 mM aqueous solution of $KAuCl_4$. The Ag-Galinstan material was prepared by adding 80 mg of Galinstan alloy to 4.9 ml of 5 mM $AgNO_3$ aqueous solution, sonicating for 30 min, and then adding 0.1 ml of 5 mg ml^{-1} PVP. The Au–Galinstan material was prepared by sonicating 200 mg of Galinstan in 5 ml of 1 mM $KAuBr_4 \cdot xH_2O$ aqueous solution for 30 min. The material that had been prepared was to be deionized.[42]

2.6 Supported catalytically active liquid metal solution (SCALMS) containing single atom catalysts (SACs)

Atomically dispersed metal catalysts have attracted great interest in catalysis owing to its unique properties. Isolated single or minor metal atoms can be anchored to the substrate by chemical bonding or spatial confinement to maximize the efficiency of atom utilization. Due to the near 100% availability of active atoms and the tunable microenvironment of the metal catalyst core, single-atom catalysts (SACs) have distinguished themselves in various catalytic fields with respect to enhanced rates, conversions and selectivity of industrial reactions.[43–52] As the majority of catalytic reactions take place on the catalyst metal surface,[53] the atoms of metal that are unable to reach the reactant molecules are largely wasted.[54] Noble metals (*e.g.* Platinum group of metals) tend to be used as superior catalysts, but with their high price and limited quantities, the proportion of these metal atoms that have no catalytically active role should be minimized.[55–57] Therefore, it is essential to explore ways to reduce the amount of precious metals used, to improve their catalytic activity and selectivity, and to increase their catalytic lifetime.[48] Employing relatively small metal particles[58] with a high surface/volume ratio and loading on specific high area support is a common solution to the above problems. For the prevention of aggregation of metal nanoparticles during catalyst synthesis or catalytic reactions, metal nanoparticles are usually dispersed into quasi-two-dimensional shapes, like immobilized on a carrier with a high specific surface area, so that the reaction molecules can reach as many metal surface atoms as possible.

Gallium, EGaIn, Galinstan in liquid state, as metal solvent, can dissolve different metals or metal salts with different solubilities, forming a single atom catalyst layer of catalytically active metal exposed to a liquid metal surface, its liquidity enables the metal atoms on the surface to flow inwards and outwards, replacing deactivated active sites with a cycle of fresh active sites, further extending the lifetime of the catalyst while expanding the contact area between the catalyst and the reactant molecules.

Platinum powder or nanoparticles in an inert gas atmosphere (in the case of the generation of oxidation layers) can be mechanically integrated with liquid metal Ga or Ga alloys (EGaIn or Galinstan) with no Pt–Pt bonding or Pt clustering observed.[59] Unique properties determine the formation of Pt SAC. There is a solubility range for virtually all precious metals and transition metals in liquid Ga. The solubility of Pt in Ga is governed by the following equation:[60]

$$\log C = A - \frac{B}{T}$$

where C is the Pt concentration in liquid Ga (at%), $A = 3.3$ and $B = 2.450$ are the solubility constants, and T is the absolute temperature.

3 Application of Ga-based liquid metals in the energy industry

The rapid development of industry has caused severe damage to the natural environment, and corresponding research has been conducted on clean energy as an alternative to traditional energy sources. Ga-based liquid metal catalysts require less energy (room temperature or relatively low temperature) than conventional thermal catalysts,[61] making them an attractive catalyst for environmental protection and clean energy applications. The formation of isolated metal sites in a liquid metal matrix permits the integration of several characteristics of multiphase catalysis (particularly the operational friendliness of product separation procedures) with those of homogeneous catalysis, as the metal sites exhibit different electronic properties due to interactions between the metals.[62] Ga–Pd liquid metal catalysts are more selective than bulk Pd catalysts in the steam reforming of methanol to hydrogen.[63]

3.1 Synthesis of ethylene by non-petroleum routes

The investigation of non-petroleum ethylene synthesis routes has been a top research priority. Conventional thermal catalysis

of ethylene frequently necessitates temperatures above 200 °C and gas pressures of 5 bars with a high hydrogen consumption, exposing the disadvantage of high production costs.[64] Armbrüster *et al.*[11,12] prepared ionic metal precursors by co-reduction in tetrahydrofuran (THF) with lithium triethyl borohydride ($LiHBEt_3$) to prepare three types of crystal structures of single-phase Ga–Pd nanoparticles (GaPd, $GaPd_2$, Ga_7Pd_3).[10] Fig. 1 depicts the instruments used to ensure the formation of intermetallic compounds during characterization. The GaPd catalyst converts constant 90% of acetylene at 473 K after 2 h, while the Ga_7Pd_3 catalyst converts 99% of constant acetylene at 473 K after 20 h. In the acetylene semihydrogenation reaction, the unloaded nanoparticles demonstrated high catalytic activity and selectivity, according to the study. Experimental results demonstrated that Ga–Pd catalysts for the semi-hydrogenation of acetylene to ethylene outperformed commercially available catalysts.

Föttinger *et al.*[42] elaborated on the formation and stability of bimetallic nanoparticles by focusing on the *in situ* characterization of functional catalysts, the study of catalysts for technological applications, and model catalysts, which provide comprehensive and complementary information on relevant atomic or molecular surface processes. Comparison with the results of a theoretical simulation (acetylene to ethylene) provides additional insight.

3.2 Alkanes to hydrogen

Catalytic hydrogen production from alkanes is a widely used method for hydrogen production due to its easy product separation and mature technology. However, alkane hydrogen production is part of the gray hydrogen industry, and its byproduct CO_2 emissions cause irreparable environmental damage. Taccardi *et al.*[65] reported a catalytically active liquid metal solution (Ga–Pd SCALMS, Ga/Pd = 1–52) loaded on porous glass with various crystal structures[10] to test the selectivity and catalytic activity pattern in butane deep dehydrogenation (BDH). Ga/Pd = 52 (molar ratio) yields the best selectivity and activity towards butane. Raman *et al.*[66] studied a Ga–Pt based liquid metal solution (Ga–Pt SCALMS) for propane dehydrogenation (PDH) loaded on a porous carrier material at temperatures between 500 °C and 600 °C. The performance of liquid metal solution was compared to that of silicon dioxide (SiO_2), aluminum oxide (Al_2O_3), and silicon carbide (SiC). It was discovered that the SCALMS loaded on the Al_2O_3 carrier exhibited significant scorch deactivation; the SCALMS loaded on SiC exhibited the best catalytic activity; and the SCALMS loaded on SiO_2 exhibited the highest stability and lowest tendency for cracking at higher temperatures, maintaining a propane selectivity of over 93% at 600 °C. Comparing SCALMS catalysts with Pt-solid-phase catalysts and Ga–Pt-solid-phase catalysts loaded on three carriers (Fig. 2), it was discovered that SCALMS loaded on SiC demonstrated the highest catalytic activity and resistance to coking loss. Redekop *et al.*[22] compared the selectivity of Pt–Ga catalysts with Pt–(Mg/Al/Ga)Ox for deep propane dehydrogenation and found that Ga-containing catalysts with Ga/Pt ratios greater than 2 were less active during the initial stages of propane dehydrogenation but more selective and less susceptible to coking than Ga-free and less Ga-containing catalysts.

3.3 Carbon dioxide to methanol

Methanol from carbon dioxide hydrogenation is a method for utilizing carbon dioxide as a resource, and the product can be used for various purposes, including liquid fuel for methanol

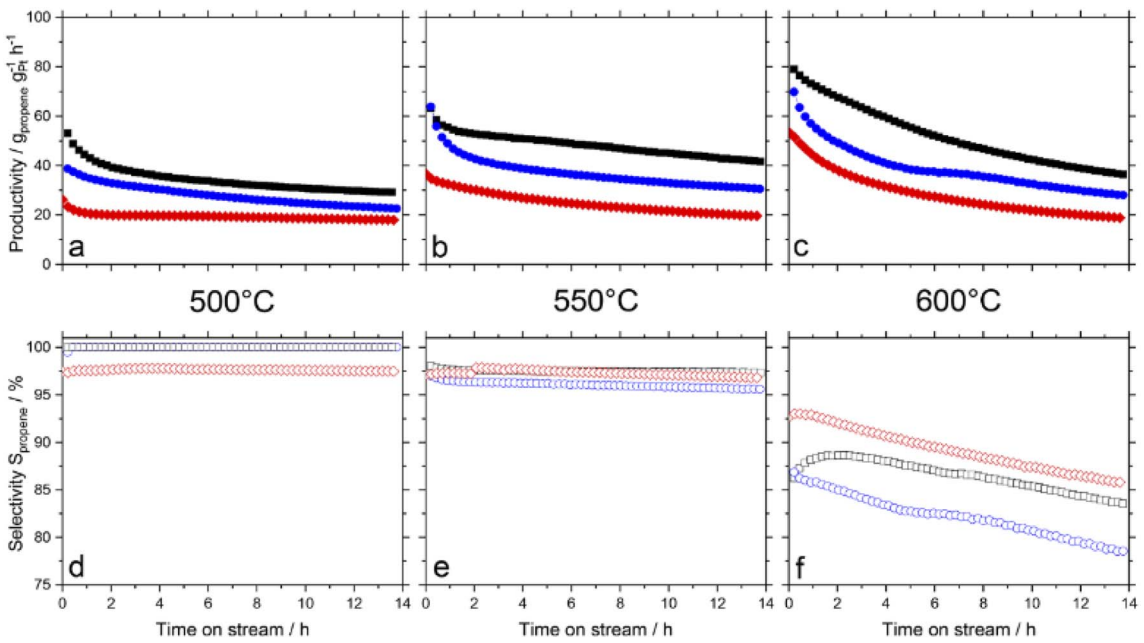

Fig. 2 SCALMS loaded with Al_2O_3 (blue), SiO_2 (red), and SiC (black) at 500–600 °C in terms of propane productivity (a–c) and catalyst selectivity (d–f).

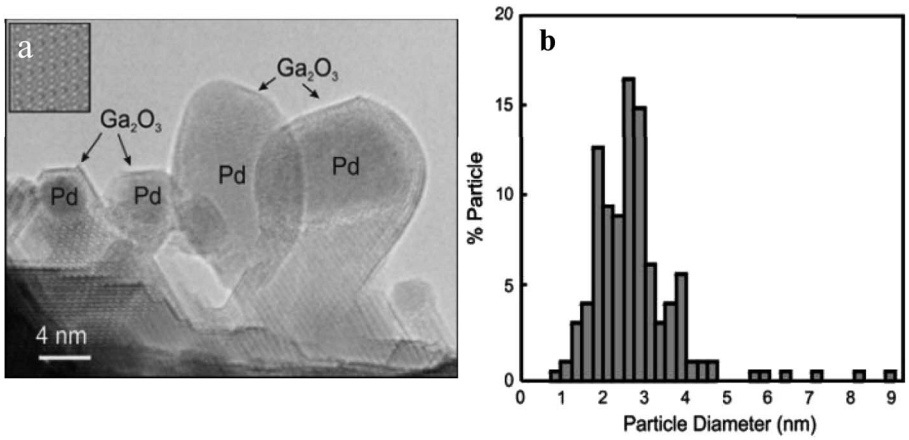

Fig. 3 (a) The HRTEM image of the Pd/β-Ga_2O_3 catalyst after reaction; (b) metal particle size distribution.

fuel cells (DMFC) and hydrogen from methanol steam reforming. Studt[67] prepared a nickel–gallium (Ni–Ga) catalyst to hydrogenate carbon dioxide to methanol at ambient pressure; the catalyst exhibited intriguing activity, selectivity, and stability for ambient pressure CO_2 reduction. The issue of carbon monoxide byproducts resulting from the reversible water–gas reaction has been resolved, and a low-pressure mini apparatus for preparing methanol from carbon dioxide has been proposed. On the basis of previous research, Nguyen *et al.*[23] investigated the effect of Ni–Ga catalyst preparation method, alloy composition ratio, and reaction temperature on the activity and stability of Ni–Ga catalysts with a focus on catalyst structure using a variety of instrumental techniques (XRD, STEM, TG-DTA, BET, XPS) to provide catalytic process overview. Men *et al.*[24] prepared HTlc precursors with 65% Ni atomic percentage and gallium equilibrium using the urea hydrolysis hydrothermal method, fabricated Ni_5Ga_3 catalysts synthesized from hydrotalc-like compounds (HTlc) precursors for CO_2 hydrogenation to methanol, and fully characterized them. The improved catalytic performance was proven by endurance tests with constant CO_2 conversion and 100% methanol selectivity at 200 °C and 0.27 s^{-1} turnover frequency.

Fujitani *et al.*[68] observed that the support had a significant effect on the catalytic activity of the Pd-based catalysts for the synthesis of methanol from CO_2 and hydrogen, with Pd/Ga_2O_3 showing a 2-fold higher yield and a 20-fold higher turnover frequency than Cu/ZnO, Collins *et al.*[69] studied the effect of palladium–gallium interactions in Pd (1wt%)/β-Ga_2O_3 during the hydrogenation of CO_2 to methanol and made a comparison with Pd/SiO_2 and pure β-Ga_2O_3 to characterize the catalyst material (Fig. 3). They discovered that Ga–Pd bimetallic microcrystals act to supply atomic hydrogen to the oxidation surface through spillover and inhibit the decomposition of methanol and carbon monoxide generation. At 3 MPa and 523 K, the Pd (1wt%)/β-Ga_2O_3 catalyst reaches a 52% methanol selectivity compared to the 12% methanol selectivity for Pd (2wt%)/SiO_2.

3.4 Methanol steam reforming to hydrogen

Methanol steam reforming manifests a relatively mild reaction condition, with an easy separation of the product and technically mature hydrogen production; the carbon dioxide in the product can be recycled in a special process to achieve zero carbon emissions when methanol is reformed with steam. Thus MSR is a highly promising process for the production of automotive hydrogen in fuel cell vehicles.[70] Li *et al.*[71] fabricated a series of gallia-supported Pd–Ga catalysts that consist of metallic nanoparticles on three porous polymorphs of Ga_2O_3 (α-, β-, and γ-Ga_2O_3) by a controlled co-precipitation of Pd and Ga. A significant effect of gallium polymorphs can be observed and the selectivity increases in the order of γ-Ga_2O_3 (20%) < α-Ga_2O_3 (30%) < β-Ga_2O_3 (40%). Lorenz[72] investigated the CO_2 selectivity of Pd–Ga_2O_3 catalysts (Ga_2O_3-supported Pd-based intermetallic phases) in methanol steam reforming and tested the catalytic performance of α-Ga_2O_3, β-Ga_2O_3 and γ-Ga_2O_3 crystalline forms as palladium oxide carriers in methanol steam reforming. Pd/β-Ga_2O_3 and Pd/γ-Ga_2O_3 appear to be similarly unselective, but Pd/α-Ga_2O_3 exhibits 85% CO_2 selectivity at 673 K (Table 1).

4 Application of Ga-based liquid metals in the environmental industry

Carbon dioxide, the most prevalent exhaust gas from the chemical industry, is also one of the most significant greenhouse gases in the Earth's atmosphere, contributing up to 25% to global warming. Thus, controlling carbon dioxide emissions from industrial sources is a crucial aspect of controlling greenhouse gases.[73] Reducing and capturing carbon dioxide and methane emissions is the key to combating global warming,[74] and carbon capture, utilization and storage (CCUS) has been studied for more than a decade.

4.1 Catalytic degradation of carbon dioxide

Conventional thermal catalysis of CO_2 necessitates a substantial amount of energy while suffering from the drawbacks of catalyst

Table 1 Summary of Ga based LMs applications on energy catalysis

Alloy species	Alloy components	Applications	Reaction conditions	Catalytic reaction equations	Performance evaluation	Ref.
Ga–Pd	Ga : Pd = 1 : 1, 1 : 2, 7 : 3 (at) Ga–Pd molar ratio > 5(5–52)	Acetylene semi-hydrogenation	200 °C	$CHCH + H_2 \xrightarrow{(Ga-Pd)} CH_2CH_2$	Ethylene selectivity 70%-78%	10–12, 42
		Butane dehydrogenation	1.1 bar 445 °C	$CH_3CH_2CH_2CH_3 \xrightarrow{(Ga-Pd)} CH_3CHCHCH_3 + H_2$	Butene-selective for 20 hours of operation 75%-80%	65
Ga–Pt	Ga : Pt = 49 : 1 (at)	Propane dehydrogenation	1.2 bar 550 °C	$CH_3CH_2CH_3 \xrightarrow{(Ga-Pt)} CH_3CHCH_2 + H_2$	Ethane selectivity >95%	66
	Ga : Pt ≈ 5.4 (at)	Propane deep dehydrogenation	101.3 kPa 600 °C	$CH_3CH_2CH_3 \xrightarrow{(Ga-Pt)} C + H_2$	Propane selectivity >98%	22
Ni–Ga	Ga : Ni = 5 : 3 (at)	Hydrogenation of CO_2 to methanol	Ambient pressure 220 °C	$CO_2 + H_2 \xrightarrow{(Ni-Ga)} CH_3OH + H_2O$	CO_2 selectivity >90%	23 and 24
	Pd (1wt%)/β-Ga_2O_3	Hydrogenation of CO_2 to methanol	0.7 MPa > 250 °C	$CO_2 + H_2 \xrightarrow{Au-Pd} CH_3OH + H_2O$	—	68 and 69
Pd-G_2O_3	Pd (10wt%)/α-Ga_2O_3 Pd (10wt%)/β-Ga_2O_3 Pd (10wt%)/γ-Ga_2O_3 Pd_2Ga/α-Ga_2O_3 Pd_2Ga/β-Ga_2O_3 Pd_2Ga/γ-Ga_2O_3 Pd_5Ga_3/α-Ga_2O_3 Pd_5Ga_3/β-Ga_2O_3 Pd_5Ga_3/γ-Ga_2O_3	Methanol steam reforming	400 °C	$CH_3OH + H_2O \xrightarrow{(Ga-Pd)} H_2 + CO_2$	CO_2 selectivity 80%	71 and 72
		Acetylene semi-hydrogenation	200 °C	$CHCH + H_2 \xrightarrow{(Pd_5Ga_3-\alpha-/\beta-/\gamma-Ga_2O_3)} CH_2CH_2$	Ethylene selectivity 74%-77%. Pd_5Ga_3/α-Ga_2O_3 > 80%	71

deactivation and oxidation. Using Ga–In liquid metal (EGaIn) and the carbon dioxide solvent dimethylformamide (DMF), Zuraiqi *et al.*[75] designed a reactor for the catalytic degradation of carbon dioxide. The reduction product was either singlet carbon or carbon monoxide, and catalyst coking deactivation did not occur between 25 °C and 500 °C. Analysis of the catalytic products and yields (Fig. 4(a and b)) as well as the catalyst prior to and after the reaction revealed that Ga in the alloy was the catalytically active material for the degradation of CO_2 and that Ga could regain catalytic activity through the reduction process after being oxidized.

Esrafilzadeh *et al.*[76] added 3 wt% cerium (cerium has a solubility of 0.1–0.5 wt% in Galinstan alloys) to the Galinstan alloy to form a layer of cerium oxide on the surface of the liquid metal to degrade CO_2 (Fig. 4(e)). The solid product composition was analyzed by XPS (Fig. 4(c)), and the Faraday efficiency was calculated. The product was determined at various potentials (Fig. 4(d)); the surface properties of the liquid metal prevented coking deactivation; the reduction of the catalyst was accomplished by applying a very low cerium reduction potential, balancing the high selectivity of the catalyst with the low energy requirement.

Tang *et al.*[77] utilized a suspension of Ga and Ag(I) as the precursors of the co-catalysts in a bubbling column reactor filled with dimethylformamide (DMF) and ethanolamine (ETA) with external ultrasonic and mechanical stirring and subjected to catalytic degradation of CO_2 at close to room temperature. In a reactor with a specific height and volume, up to 92% of 8SCCM CO_2 was converted into singlet carbon, oxygen, and gallium oxide (Fig. 5). The total reaction was as follows:

$$Ga + CO_2 \rightarrow Ga^+ + CO_2^- \quad (1)$$

$$Ga + CO_2^- \rightarrow Ga^+ + CO + O_2^- \quad (2)$$

$$2Ga + CO \rightarrow 2Ga^+ + C + O_2^- \quad (3)$$

$$2O^{2-} \rightarrow O_2 + 4e^- \quad (4)$$

The addition of silver ions permits the reduction of oxidized Ga to catalytically active Ga monomers *via* the following pathway:

$$4Ga^+ + 4Ag_{0.72}Ga_{0.28} \rightarrow 4Ga + 4Ag_{0.72}Ga_{0.28}{}^+ \quad (5)$$

$$4Ag_{0.72}Ga_{0.28}{}^+ + 4e^- \rightarrow 4Ag_{0.72}Ga_{0.28} \quad (6)$$

Due to the density difference between carbon and metallic compounds, carbon sheets naturally float on the reactor's surface. The operational costs of CO_2 capture and conversion using DMF + ETA are lower than those of any other state-of-the-art technology, according to general estimates based on current electricity costs.

4.2 Catalytic degradation of organic methylene blue in wastewater

Methylene blue (MB) is a biotoxic, teratogenic, carcinogenic, and mutagenic organic cationic dye that is frequently found in

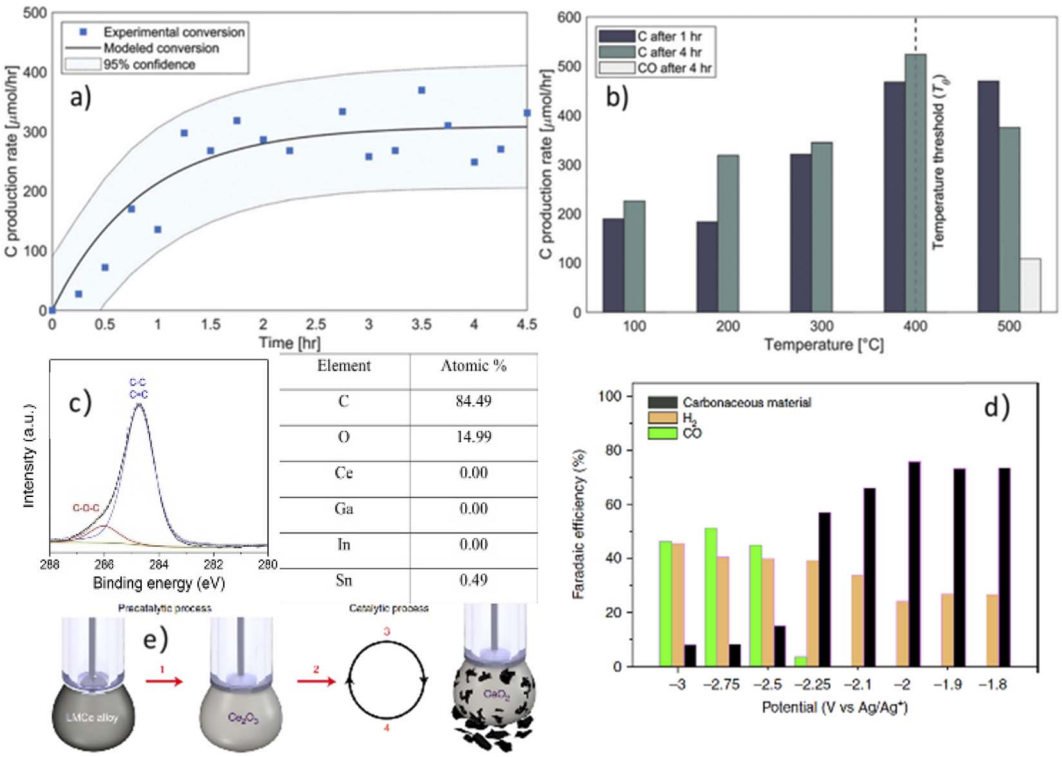

Fig. 4 Performance evaluation of EGaIn alloys. (a) Carbon production rate with a continuous pass of CO_2 to the bubble tower reactor at 200 °C and ambient pressure; (b) reduction product rate with a continuous pass of CO_2 at different temperatures; (c) XPS analysis of solid product elemental composition; (d) Faraday efficiency product diagram; (e) Schematic diagram of Ce-Galinstan catalysis.

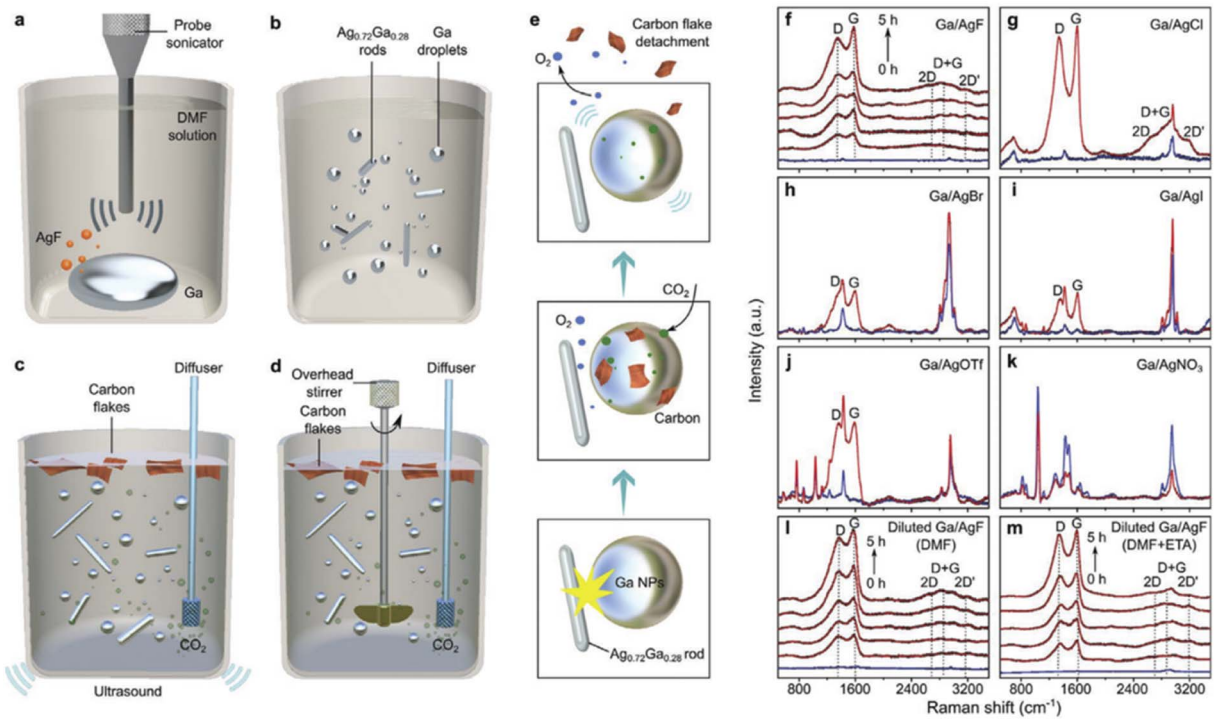

Fig. 5 Schematics and Raman spectra of solid carbon produced from CO_2 using liquid metal. (a–d) Schematic illustrations for preparing a suspension of the catalyst (a and b) and the CO_2 reduction process (c and d) using various mechanical energy inputs. (e) A schematic illustration of the CO_2 conversion process. The formation/detachment of the carbon flakes and the generation/escape of O_2 are indicated. (f–k) Raman spectra of the samples obtained from the reaction mixes of Ga with various silver salts as precursors in DMF: (f) AgF (*vs.* time), (g) AgCl, (h) AgBr, (i) AgI, (j) AgOTf, and (k) $AgNO_3$. The D and G bands at 1350 cm^{-1} and 1600 cm^{-1}, respectively, emerged after the reactions occur. (l and m) Raman spectra (*vs.* time) from mixture surfaces from the ten-times diluted reaction system (Ga and AgF mix) by employing DMF (l) and DMF + ETA (m) as the reaction solutions. The blue and red curves in (f)–(m) are the respective Raman spectra for the samples before and after reaction.

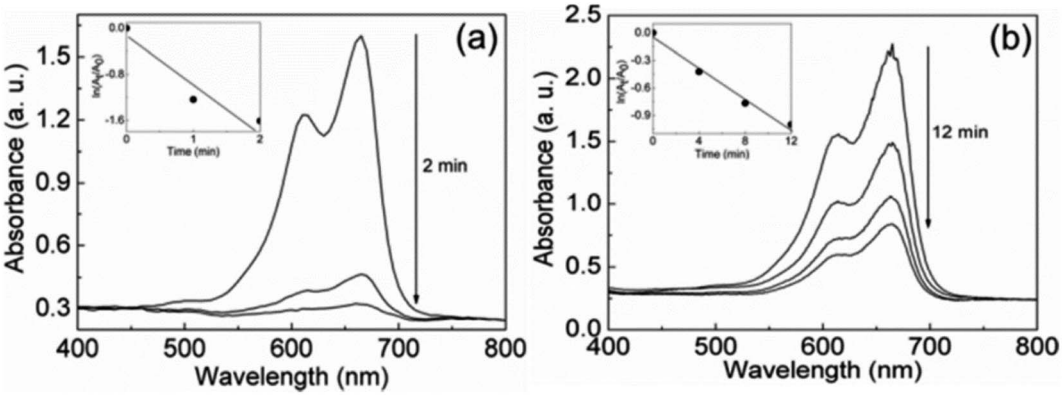

Fig. 6 Time-dependent UV-Vis absorption spectra of the reduction of 7.2×10^{-5} M methylene blue by excess $NaBH_4$ in the presence of (a) Ag–Galinstan and (b) Au–Galinstan catalysts.

Table 2 Summary of Ga based LMs applications on environmental catalysis

Alloy species	Alloy components	Applications	Reaction conditions	Catalytic reaction equations	Ref.
EGaIn	Ga : In = 75%:25% (wt%)	CO_2 catalytic degradation	25–500 °C	$CO_2 \xrightarrow{Ga-In} C + Ga_2O_3$	75
Ce-Galinstan	Ce:3 wt% Ga:68.5 wt% In:21.5 wt% Sn:10 wt%	CO_2 catalytic degradation	Room temperature	$CO_2 \xrightarrow{Ce-GaInSn} C + Ce_2O_3$	76
Ag–Ga	AgF : Ga = 1.0–7.0 (wt%) Ag : Ga = 0.72 : 0.28 (at)	CO_2 catalytic degradation	Near room temperature	$CO_2 \xrightarrow{Ag-Ga} C + Ga_2O_3$ $4Ga^+ + 4Ag_{0.72}Ga_{0.28} \rightarrow 4Ga^+4Ag_{0.72}Ga_{0.28}{}^+$ $4Ag_{0.72}Ga_{0.28}{}^+ + 4e^- \rightarrow 4Ag_{0.72}Ga_{0.28}$	77
Au/Ag-Galinstan	—	Methylene blue catalytic degradation	—	$MB^+ \xrightarrow{Ag/Au-GaInSn} MB$	42
Cu/W/Mo/Ni-EGaIn	Cu/W/Mo/Ni : EGaIn (75.5 : 24.5wt%) = 15 : 85 (wt%)	Methylene blue and Congo red catalytic degradation	Photocatalysis	—	78

the wastewater of the printing and dyeing industries. Often, MB-contaminated waters have a high chromaticity and abundant chemical oxygen demand (COD). Hoshyargar *et al.*[42] prepared a liquid metal core/solid metal shell Au/Ag-GaInSn nanoparticle for the electrical replacement of Galinstan using gold (Au) and silver (Ag). The nanoparticles' catalytic activity against MB in the presence of sodium borohydride was evaluated (Fig. 6). During contact with the reduction medium, the morphology of the Au–Galinstan catalyst changed to micron-sized spherical particles decorated with Ag nanoparticles, whereas the morphology of the Ag–Galinstan catalyst remained unchanged. The composition of the catalyst also changed, with a significantly lower gallium concentration (~3%), and a 2 : 1 ratio of indium (In) to tin(Sn) in Ag–Galinstan. Therefore, the Ag and Au nanomaterials facilitate two electron transfer processes between BH^{4-} and MB^+, thereby enhancing the electron capacity of the catalyst. Tang *et al.* prepared a Ga–Pt liquid metal catalyst containing Pt nanoparticles dissolved in Ga to test the catalytic activity in comparison to the commercial Pt/C catalyst in MB degradation. Ga–Pt catalyst is approximately 84 times more active than commercial Pt/C catalyst. Moreover, based on the ratio of surface Pt atoms in Ga–Pt and Pt/C (Ga–Pt : Pt/C = $\sim 8.6 \times 10^{-5}$), it is estimated that the activity of Pt atoms in the Ga–Pt system is more than five orders of magnitude greater than that of Pt/C. Liang *et al.*[78] proposed a liquid metal/metal oxide core–shell heterostructure catalyst. The liquid metal was chemically modified with Cu/W/Mo/Ni metal nanoparticles forming Ga_2O_3 core–shell heterostructure catalysts and applied to photocatalytic degradation of organic pollutant (methylene blue and congo red) stock solution. The degradation of methylene blue and congo red by Ni-LM catalyst was found to be 92% and 79%, respectively (Table 2).

5 Discussions

The worldwide energy crisis is monumental. To meet the escalating energy demand and develop sustainable energy sources, it is urgent to make revolutionary cost and scalability advancements. Scalability becomes the deciding factor between research and industrial applications in the same phase when designing application-specific processes such as hydrogen

economy and sustainable energy solutions, which must operate on large scales inevitably. Central to scalability considerations is the intersection between cost, large-scale processing, ease of fabrication, and ensuring a stable supply of materials. In summary, Ga-based liquid metal catalysts have relatively low viscosity, which allows the active sites on liquid surface to be regenerated spontaneously with the Ga atoms flow in the liquid, or by designing a bubbler-type reactor with gas bubbles as the driving force for the Ga atoms flow, resulting in far more theoretical active sites than conventional solid catalysts and a significantly longer catalyst lifetime. As a metal solvent, Gallium, EGaIn or Galinstan are capable of solubilizing almost all noble metals and transition metals, whereas it has been reported that specific metal oxides show a certain solubility in liquid Ga alloys, however, the species of metal oxides that can be solubilized are not clear yet. To ensure the scalability of LM catalysts in energy applications, the selection of metals must be restricted to those that are abundant and inexpensive. In addition, Ga is relatively inexpensive in bulk at absolute atmospheric pressure compared to several solvents for industrial applications, such as ionic liquids, and it is also a relatively abundant element in the earth's crust. Although mercury is a relatively inexpensive metal, its high toxicity clearly prevents it from being utilized. Overall, it is anticipated that the maturity of the metal economy and the excellent recoverability of metal will result in the expansion of LM-catalyzed processes. LMs have been successfully implemented in large commercial processes to date. Consequently, even though LM catalysis is still an emerging field, operational knowledge from these applications can be applied to the development of scalable breakthroughs in LM catalysis to ensure optimal production levels at low costs. At this stage, the research of liquid metal catalysts focuses primarily on the following aspects:

(1) In alkane dehydrogenation, additional modulation of reaction conditions and adjustment of metal components may be attempted to enhance the catalytic performance of various alkane selectivity.

(2) To avoid and reduce the use and even the waste of precious metals, research on methods to recover precious metals from liquid metals and the improvement of catalyst performance should be expanded, thereby preventing the use of various metals in liquid metal alloys.

Catalysts based on liquid metal materials, such as room temperature liquid metal catalysts (EGaIn, Galinstan), bimetallic-liquid metal catalysts, polymetallic-liquid metal catalysts, and liquid metal multiphase catalysts, offer new opportunities for the advancement of catalytic science and engineering and provide new catalytic routes for a wide range of existing industrial catalysis. Among the catalytic reactions for which liquid metal catalysts hold promise is:

(1) The metals utilized in cutting-edge metal hydrogen storage technology are typically reactive. Ga and these reactive metals can form an alloy that will protect these metals while preserving their properties, since the surface of liquid Ga can form a dense oxide layer that prevents air and water vapor from reacting further with the metal.

(2) It is unknown whether the products of CO_2 catalytic degradation can be converted into chemicals with added value *via* hydrogenation or other methods.

(3) It must be determined if additional metals can be added to Ga, EGaIn, and Galinstan to create polymetallic catalysts that can be used for more energy- and environment-friendly catalytic reactions.

(4) The organically polluted wastewater contains a variety of contaminants. It is possible to study the selectivity and catalytic performance of various liquid metals for various organic pollutants, including photocatalysis and electrocatalysis.

(5) SAC in SCALMS as an emerging research highlight await further exploration by researchers, covering fabrication methodologies, component regulation, potential catalytic reaction species and mechanisms that can lead to better performance than bulk metal catalysts.

Briefly, previous research on LM catalysts has demonstrated their multidisciplinary potential. Researchers believe that Ga-based liquid metal catalysts will soon provide new catalytic routes for a variety of applications, thereby expanding the scope of catalytic chemistry.

6 Conclusions

This review presents a selection of typical research results on liquid metal catalysts and describes significant research on the use of liquid metal materials in catalytic applications over the past 15 years. With its low viscosity and liquid properties, the liquid metal enables the catalytic active sites to continuously regenerate, thereby extending the catalyst's lifetime prior to deactivation and making it more resistant to overall catalyst deactivation caused by deactivation of the active sites on the surface of the solid catalyst. In addition to nearly all precious and transition metals having a reasonable solubility in liquid Ga, liquid–gas phase gases also have a certain solubility. Environmental and energy catalysis are the two main application sectors for LM catalysts. Several practical applications are also discussed, including catalysis for the synthesis of ethylene *via* non-petroleum routes, alkane dehydrogenation, CO_2 hydrogenation to methanol, and catalytic degradation of CO_2. In addition, a summary of the various performance evaluations of Pd, Pt, and Ni alloys with Ga/Ga oxides, EGaIn/Galinstan with Au and Ag under multiple metal components and reaction conditions is provided. It has been demonstrated that liquid metal catalysts play an important role in enhancing the efficiency of chemical reactions and can be utilized in a variety of fields, and significant progress has been made. However, research on liquid metal catalysts is still in its infancy, and challenges such as how to form different metal types with different catalytic activities on the surface of liquid metal and the application of liquid metal catalysts in a variety of fields are yet to be resolved.

Conflicts of interest

There are no conflicts to declare.

Acknowledgements

This work was supported by the Liaoning Revitalization Talents Program (XLYC1907075).

References

1 Q. Wang, Y. Yu and J. Liu, *Adv. Eng. Mater.*, 2018, **20**, 1700781.
2 Y. Lu, Q. Hu, Y. Lin, D. B. Pacardo, C. Wang, W. Sun, F. S. Ligler, M. D. Dickey and Z. Gu, *Nat. Commun.*, 2015, **6**, 1–10.
3 M. D. Dickey, R. C. Chiechi, R. J. Larsen, E. A. Weiss, D. A. Weitz and G. M. Whitesides, *Adv. Funct. Mater.*, 2008, **18**, 1097–1104.
4 R. E. Calabrese, E. Bury, F. Haque, A. Koh and C. Park, *Composites, Part B*, 2022, **234**, 109686.
5 K. B. Ozutemiz, J. Wissman, O. B. Ozdoganlar and C. Majidi, *Adv. Mater. Interfaces*, 2018, **5**, 1701596.
6 W. Yu, M. D. Porosoff and J. G. Chen, *Chem. Rev.*, 2012, **112**, 5780–5817.
7 Y. Lin, J. Genzer and M. D. Dickey, *Adv. Sci.*, 2020, **7**, 2000192.
8 D. Wang, X. Wang and W. Rao, *Acc. Mater. Res.*, 2021, **2**, 1093–1103.
9 M. H. Malakooti, M. R. Bockstaller, K. Matyjaszewski and C. Majidi, *Nanoscale Adv.*, 2020, **2**, 2668–2677.
10 H. Okamoto, *J. Phase Equilib. Diffus.*, 2008, **29**, 466.
11 M. Armbrüster, G. Wowsnick, M. Friedrich, M. Heggen and R. Cardoso-Gil, *J. Am. Chem. Soc.*, 2011, **133**, 9112–9118.
12 M. Armbrüster, K. Kovnir, M. Behrens, D. Teschner, Y. Grin and R. Schlögl, *J. Am. Chem. Soc.*, 2010, **132**, 14745–14747.
13 Y. C. Cao and X. Z. Jiang, *J. Mol. Catal. A: Chem.*, 2005, **242**, 119–128.
14 V. Ponec, *Appl. Catal., A*, 1997, **149**, 27–48.
15 W. Tuley and R. Adams, *J. Am. Chem. Soc.*, 1925, **47**, 3061–3068.
16 D. Richard, J. Ockelford, A. Giroir-Fendler and P. Gallezot, *Catal. Lett.*, 1989, **3**, 53–58.
17 O. Alexeev and B. Gates, *Ind. Eng. Chem. Res.*, 2003, **42**, 1571–1587.
18 S. Gőbölös, J. L. Margitfalvi, M. Hegedűs and Y. A. Ryndin, *React. Kinet. Catal. Lett.*, 2006, **87**, 313–324.
19 Y. Nakaya, F. Xing, H. Ham, K. i. Shimizu and S. Furukawa, *Angew. Chem.*, 2021, **133**, 19867–19871.
20 A. Plomp, D. Van Asten, A. Van der Eerden, P. Mäki-Arvela, D. Y. Murzin, K. De Jong and J. Bitter, *J. Catal.*, 2009, **263**, 146–154.
21 T. Romero, B. Arenas, E. Perozo, C. Bolivar, G. Bravo, P. Marcano, C. Scott, M. P. Zurita and J. Goldwasser, *J. Catal.*, 1990, **124**, 281–285.
22 E. A. Redekop, V. V. Galvita, H. Poelman, V. Bliznuk, C. Detavernier and G. B. Marin, *ACS Catal.*, 2014, **4**, 1812–1824.
23 H. K. D. Nguyen, T. H. Dang, N. L. T. Nguyen, H. T. Nguyen and N. T. Dinh, *Can. J. Chem. Eng.*, 2018, **96**, 832–837.
24 Y. Men, X. Fang, Q. Gu, R. Singh, F. Wu, D. Danaci, Q. Zhao, P. Xiao and P. A. Webley, *Appl. Catal., B*, 2020, **275**, 119067.
25 G. Wagner and W. Gitzen, *J. Chem. Educ.*, 1952, **29**, 162.
26 J. W. Boley, E. L. White and R. K. Kramer, *Adv. Mater.*, 2015, **27**, 2355–2360.
27 A. Kwong and Z. Munir, *J. Less-Common Met.*, 1973, **30**, 387–395.
28 L. E. Felton, C. H. Raeder and D. B. Knorr, *JOM*, 1993, **45**, 28–32.
29 A. Burdakin, B. Khlevnoy, M. Samoylov, V. Sapritsky, S. Ogarev, A. Panfilov, G. Bingham, V. Privalsky, J. Tansock and T. Humpherys, *Metrologia*, 2008, **45**, 75.
30 C. Tabor, S. Holcomb and J. Heikenfeld, *Adv. Mater. Interfaces*, 2020, **7**, 1902182.
31 C. Chiew, M. Morris and M. H. Malakooti, *Mater. Adv.*, 2021, **2**, 7799–7819.
32 N. Morley, J. Burris, L. Cadwallader and M. Nornberg, *Rev. Sci. Instrum.*, 2008, **79**, 056107.
33 W. Zhang, N. Srichan, A. F. Chrimes, M. Taylor, K. J. Berean, J. Z. Ou, T. Daeneke, A. P. O'Mullane, G. Bryant and K. Kalantar-zadeh, *Sens. Actuators, B*, 2016, **223**, 52–58.
34 A. Fassler and C. Majidi, *Lab Chip*, 2013, **13**, 4442–4450.
35 Z. J. Farrell and C. Tabor, *Langmuir*, 2018, **34**, 234–240.
36 A. Refaat, *Int. J. Environ. Sci. Technol.*, 2011, **8**, 203–221.
37 Y. Song, X. Li, L. Sun and L. Wang, *RSC Adv.*, 2015, **5**, 7267–7279.
38 C. Ray and T. Pal, *J. Mater. Chem. A*, 2017, **5**, 9465–9487.
39 S. T. Kochuveedu, Y. H. Jang and D. H. Kim, *Chem. Soc. Rev.*, 2013, **42**, 8467–8493.
40 W. Zhang, J. Z. Ou, S. Y. Tang, V. Sivan, D. D. Yao, K. Latham, K. Khoshmanesh, A. Mitchell, A. P. O'Mullane and K. Kalantar-zadeh, *Adv. Funct. Mater.*, 2014, **24**, 3799–3807.
41 R. David and N. Miki, *Nanoscale*, 2019, **11**, 21419–21432.
42 F. Hoshyargar, J. Crawford and A. P. O'Mullane, *J. Am. Chem. Soc.*, 2017, **139**, 1464–1471.
43 R. Lang, W. Xi, J.-C. Liu, Y.-T. Cui, T. Li, A. F. Lee, F. Chen, Y. Chen, L. Li and L. Li, *Nat. Commun.*, 2019, **10**, 1–10.
44 J. Lin, A. Wang, B. Qiao, X. Liu, X. Yang, X. Wang, J. Liang, J. Li, J. Liu and T. Zhang, *J. Am. Chem. Soc.*, 2013, **135**, 15314–15317.
45 S. Yang, J. Kim, Y. J. Tak, A. Soon and H. Lee, *Angew. Chem., Int. Ed.*, 2016, **55**, 2058–2062.
46 Z. Jakub, J. Hulva, M. Meier, R. Bliem, F. Kraushofer, M. Setvin, M. Schmid, U. Diebold, C. Franchini and G. S. Parkinson, *Angew. Chem.*, 2019, **131**, 14099–14106.
47 Y. Ren, Y. Tang, L. Zhang, X. Liu, L. Li, S. Miao, D. Sheng Su, A. Wang, J. Li and T. Zhang, *Nat. Commun.*, 2019, **10**, 1–9.
48 Z. Zhang, J. Liu, J. Wang, Q. Wang, Y. Wang, K. Wang, Z. Wang, M. Gu, Z. Tang and J. Lim, *Nat. Commun.*, 2021, **12**, 1–9.
49 Z.-Y. Wu, M. Karamad, X. Yong, Q. Huang, D. A. Cullen, P. Zhu, C. Xia, Q. Xiao, M. Shakouri and F.-Y. Chen, *Nat. Commun.*, 2021, **12**, 1–10.
50 Z. Du, X. Chen, W. Hu, C. Chuang, S. Xie, A. Hu, W. Yan, X. Kong, X. Wu and H. Ji, *J. Am. Chem. Soc.*, 2019, **141**, 3977–3985.
51 N. Zhang, X. Zhang, L. Tao, P. Jiang, C. Ye, R. Lin, Z. Huang, A. Li, D. Pang and H. Yan, *Angew. Chem., Int. Ed.*, 2021, **60**, 6170–6176.

52 K. L. Zhou, Z. Wang, C. B. Han, X. Ke, C. Wang, Y. Jin, Q. Zhang, J. Liu, H. Wang and H. Yan, *Nat. Commun.*, 2021, **12**, 1–10.
53 B. L. Hendriksen, M. D. Ackermann, R. Van Rijn, D. Stoltz, I. Popa, O. Balmes, A. Resta, D. Wermeille, R. Felici and S. Ferrer, *Nat. Chem.*, 2010, **2**, 730–734.
54 K. Foger, in *Catalysis*, Springer, 1984, pp. 227–305.
55 J. Liu, *ACS Catal.*, 2017, **7**, 34–59.
56 J. r. m. D. Pelletier and J.-M. Basset, *Acc. Chem. Res.*, 2016, **49**, 664–677.
57 F. R. Lucci, J. Liu, M. D. Marcinkowski, M. Yang, L. F. Allard, M. Flytzani-Stephanopoulos and E. C. H. Sykes, *Nat. Commun.*, 2015, **6**, 1–8.
58 A. K. Datye, *Nat. Nanotechnol.*, 2019, **14**, 817–818.
59 M. A. Rahim, J. Tang, A. J. Christofferson, P. V. Kumar, N. Meftahi, F. Centurion, Z. Cao, J. Tang, M. Baharfar, M. Mayyas, F.-M. Allioux, P. Koshy, T. Daeneke, C. F. McConville, R. B. Kaner, S. P. Russo and K. Kalantar-Zadeh, *Nat. Chem.*, 2022, 1–7.
60 T. Daeneke, K. Khoshmanesh, N. Mahmood, I. A. De Castro, D. Esrafilzadeh, S. Barrow, M. Dickey and K. Kalantar-Zadeh, *Chem. Soc. Rev.*, 2018, **47**, 4073–4111.
61 X. Guo, L. Zhang, Y. Ding, J. B. Goodenough and G. Yu, *Energy Environ. Sci.*, 2019, **12**, 2605–2619.
62 S. Furukawa and T. Komatsu, *ACS Catal.*, 2017, **7**, 735–765.
63 M. Armbrüster, M. Behrens, F. Cinquini, K. Föttinger, Y. Grin, A. Haghofer, B. Klötzer, A. Knop-Gericke, H. Lorenz and A. Ota, *ChemCatChem*, 2012, **4**, 1048–1063.
64 S. Wang, K. Uwakwe, L. Yu, J. Ye, Y. Zhu, J. Hu, R. Chen, Z. Zhang, Z. Zhou and J. Li, *Nat. Commun.*, 2021, **12**, 1–9.
65 N. Taccardi, M. Grabau, J. Debuschewitz, M. Distaso, M. Brandl, R. Hock, F. Maier, C. Papp, J. Erhard and C. Neiss, *Nat. Chem.*, 2017, **9**, 862–867.
66 N. Raman, M. Wolf, M. Heller, N. Heene-Würl, N. Taccardi, M. Haumann, P. Felfer and P. Wasserscheid, *ACS Catal.*, 2021, **11**, 13423–13433.
67 F. Studt, I. Sharafutdinov, F. Abild-Pedersen, C. F. Elkjær, J. S. Hummelshøj, S. Dahl, I. Chorkendorff and J. K. Nørskov, *Nat. Chem.*, 2014, **6**, 320–324.
68 T. Fujitani, M. Saito, Y. Kanai, T. Watanabe, J. Nakamura and T. Uchijima, *Appl. Catal., A*, 1995, **125**, L199–L202.
69 S. E. Collins, J. J. Delgado, C. Mira, J. J. Calvino, S. Bernal, D. L. Chiavassa, M. A. Baltanás and A. L. Bonivardi, *J. Catal.*, 2012, **292**, 90–98.
70 J. Kang, Y. Song, T. Kim and S. Kim, *Int. J. Hydrogen Energy*, 2021.
71 L. Li, B. Zhang, E. Kunkes, K. Föttinger, M. Armbrüster, D. S. Su, W. Wei, R. Schlögl and M. Behrens, *ChemCatChem*, 2012, **4**, 1764–1775.
72 H. Lorenz, R. Thalinger, E.-M. Köck, M. Kogler, L. Mayr, D. Schmidmair, T. Bielz, K. Pfaller, B. Klötzer and S. Penner, *Appl. Catal., A*, 2013, **453**, 34–44.
73 J. F. D. Tapia, J.-Y. Lee, R. E. Ooi, D. C. Foo and R. R. Tan, *Sustainable Prod. Consumption*, 2018, **13**, 1–15.
74 K. Jiang, P. Ashworth, S. Zhang, X. Liang, Y. Sun and D. Angus, *Renewable Sustainable Energy Rev.*, 2020, **119**, 109601.
75 K. Zuraiqi, A. Zavabeti, J. Clarke-Hannaford, B. J. Murdoch, K. Shah, M. J. Spencer, C. F. McConville, T. Daeneke and K. Chiang, *Energy Environ. Sci.*, 2022, **15**(2), 595–600.
76 D. Esrafilzadeh, A. Zavabeti, R. Jalili, P. Atkin, J. Choi, B. J. Carey, R. Brkljača, A. P. O'Mullane, M. D. Dickey and D. L. Officer, *Nat. Commun.*, 2019, **10**, 1–8.
77 J. Tang, J. Tang, M. Mayyas, M. B. Ghasemian, J. Sun, M. A. Rahim, J. Yang, J. Han, D. J. Lawes and R. Jalili, *Adv. Mater.*, 2022, **34**, 2105789.
78 S. Liang, C. Wang, F. Li and G. Song, *Catalysts*, 2021, **11**, 1419.